

Progressive Glass Segmentation

Letian Yu*, Haiyang Mei*, Wen Dong, Ziqi Wei, Li Zhu, Yuxin Wang, and Xin Yang†

Abstract—Glass is very common in the real world. Influenced by the uncertainty about the glass region and the varying complex scenes behind the glass, the existence of glass poses severe challenges to many computer vision tasks, making glass segmentation as an important computer vision task. Glass does not have its own visual appearances but only transmit/reflect the appearances of its surroundings, making it fundamentally different from other common objects. To address such a challenging task, existing methods typically explore and combine useful cues from different levels of features in the deep network. As there exists a characteristic gap between level-different features, *i.e.*, deep layer features embed more high-level semantics and are better at locating the target objects while shallow layer features have larger spatial sizes and keep richer and more detailed low-level information, fusing these features naively thus would lead to a sub-optimal solution. In this paper, we approach the effective features fusion towards accurate glass segmentation in two steps. First, we attempt to bridge the characteristic gap between different levels of features by developing a Discriminability Enhancement (DE) module which enables level-specific features to be a more discriminative representation, alleviating the features incompatibility for fusion. Second, we design a Focus-and-Exploration Based Fusion (FEFB) module to richly excavate useful information in the fusion process by highlighting the common and exploring the difference between level-different features. Combining these two steps, we construct a Progressive Glass Segmentation Network (PGSNet) which uses multiple DE and FEFB modules to progressively aggregate features from high-level to low-level, implementing a coarse-to-fine glass segmentation. In addition, we build the first home-scene-oriented glass segmentation dataset for advancing household robot applications and in-depth research on this topic. Extensive experiments demonstrate that our method outperforms 26 cutting-edge models on three challenging datasets under four standard metrics. The code and dataset will be made publicly available.

Index Terms—Glass segmentation, fusion strategy, dataset, deep neural network.

I. INTRODUCTION

GLASS is commonly presented in daily-life scenes, *e.g.*, window panes, glass doors/walls, and glass guardrails, as practical and decorative usages. Yet, glass confuses many vision systems due to its transparency and invisibility [1]–[4]. For example, a drone may crash into glass surfaces without the ability to sense the presence of glass, and the navigation

Letian Yu, Haiyang Mei, Wen Dong, Yuxin Wang, Xin Yang are with the School of Computer Science and Technology at Dalian University of Technology, Dalian, 116024, China. E-mail: letianyu@mail.dlut.edu.cn; mhy666@mail.dlut.edu.cn; dongwen@mail.dlut.edu.cn; wyx@dlut.edu.cn; xinyang@dlut.edu.cn.

Ziqi Wei is with the School of Software at Tsinghua University, Beijing, 100084, China. E-mail: weizq_ruc@foxmail.com.

Li Zhu is with the School of Control Science and Engineering at Dalian University of Technology, Dalian, 116024, China. E-mail: zhuli@dlut.edu.cn.

* Letian Yu and Haiyang Mei are the joint first authors.

† Ziqi Wei and Xin Yang are the corresponding authors.

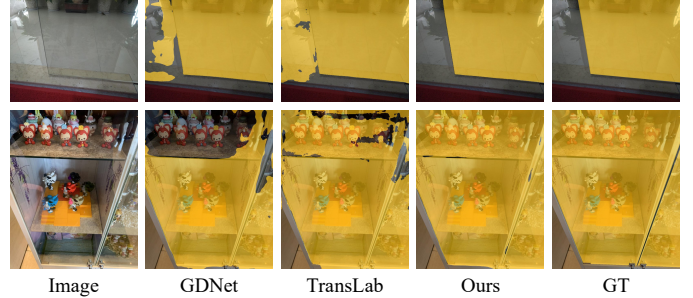


Fig. 1. Visual examples of glass segmentation. While the state-of-the-art method GDNet [2] and TransLab [3] explore large-field contextual features and boundary cues, respectively, the simple fusion between level-different features (*i.e.*, element-wise multiplication or channel-wise concatenation) ignores the characteristic gap between features, and thus leading to a sub-optimal solution (2nd and 3rd columns). In contrast, by adopting our proposed features fusion strategy, our method is able to accurately segment the glass (4th column).

robots also need to avoid bumping into the glass-like objects. Thus, the ability to segment glass is essential for AI agents in many practical applications. Automatic glass segmentation is a challenging task as glass does not have its own visual appearances but only transmit/reflect the appearances of its surroundings and thus has no relatively fixed semantics/patterns, salient features, or contrastive features [5], making it fundamentally different from other common/salient/mirror object detection/segmentation problems.

Just as human beings typically leverage different cues to identify the existence of glass, existing glass/transparency segmentation methods mainly focus on the exploration of useful information from different levels of features in the deep network, *e.g.*, both high-level and low-level large-field contextual features [2], boundary cues [4], and transformer [6] based global contexts [4]. However, the obtained cues/features typically vary in level and characteristic, *i.e.*, deep layer features in the network usually embed more high-level semantic knowledge and contextual relations and are better at locating the target objects while shallow layer features have larger spatial sizes and keep richer and more detailed low-level information such as edges, lines, and corners, and thus naively combine them (*e.g.*, channel-wise concatenation or element-wise multiplication/addition) for final segmentation would lead to a sub-optimal solution (Figure 1, 2nd and 3rd columns).

In this paper, we emphasize the *significance of the effective fusion* between different levels of features towards accurate glass segmentation. Specifically, we approach the effective level-different features fusion in two steps. First, we attempt to bridge the characteristic gap between different levels of features by developing a Discriminability Enhancement (DE) module which enables level-specific features to be

a more discriminative representation, alleviating the features incompatibility for fusion. Second, we design a Focus-and-Exploration Based Fusion (FEBF) module to achieve the goal of richly excavating useful information by simultaneously highlighting the common and exploring the difference between level-different features in the fusion process. Combining these two steps, we construct a **Progressive Glass Segmentation Network (PGSNet)** which combines multiple DE and FEBF modules to progressively aggregate features from high-level to low-level, implementing a coarse-to-fine glass segmentation. In addition, we build the first home-scene-oriented glass segmentation dataset for advancing household robot applications and in-depth research on this topic. To sum up, the main contributions of this work are as follows:

- First, we develop a novel features fusion strategy which first bridges the characteristic gap between level-different features by the proposed discriminability enhancement (DE) module and then fuses features via the well-designed focus-and-exploration based fusion (FEBF) module.
- Second, we construct a progressive glass segmentation network (PGSNet), which leverages our proposed features fusion strategy to progressively aggregate features from high-level to low-level, implementing a coarse-to-fine glass segmentation.
- Third, we build the first home-scene-oriented (HSO) glass segmentation dataset, laying a foundation for further research and household robot applications.
- Fourth, we achieve state-of-the-art glass segmentation performance on our HSO dataset as well as existing two benchmark datasets. Experimental results demonstrate the effectiveness of our method.

II. RELATED WORK

In this section, we first briefly review state-of-the-art detection/segmentation methods in different fields, including semantic segmentation, salient object detection, as well as specific region segmentation, and then discuss some representative works on deep feature fusion.

A. Semantic Segmentation

Semantic Segmentation classifies and assigns a semantic label to each pixel in an image. Recently, great progress has been achieved benefited by the advances of deep neural networks. Based on fully convolutional networks (FCNs) [7], state-of-the-art methods focus on the exploration of contextual information in different scales/levels and forms [8]–[18]. A more comparative survey [19] about methods and performances for segmentation has been proposed, grouped into 10 categories, for example, encoder-decoder based models, multi-scale and pyramid network based models and attention-based models. The glass segmentation problem we strive to address differs from semantic segmentation in that the large intra-class variation, *i.e.*, arbitrary categories of objects could appear behind the glass. Hence, treating glass as an additional semantic category fails to produce satisfactory results as the visible glass content is further semantically classified [2]. In

this paper, we also exploit different levels of features, but further employ a novel level-different features fusion strategy for accurate glass segmentation.

B. Salient Object Detection

Salient Object Detection (SOD) aims to identify the most visually distinctive object(s) in an image of a scene. Hundreds of SOD methods have been proposed in the past decades. Early methods mainly rely on the handcrafted low-level features and heuristic priors such as color [20] and contrast [21]. These features, however, have limited capability to distinguish the salient and non-salient objects, thus the approaches based on them often fail in complex scenes. Recently, state-of-the-art solutions employ convolutional neural networks (CNNs) to exploit different learning strategies and cues such as multi-level feature exploration [22]–[27], recurrent and iterative learning strategies [28]–[31], attention mechanisms [32]–[36], and edge/boundary cues [37]–[39]. Some context-aware methods [40], [41] are also discussed in SOD fields. Since glass regions and the content behind the glass surface are not always salient, SOD methods, however, cannot directly address glass segmentation due to a lack of salient features. Giving a complete review on SOD is beyond the scope of this work. We refer readers to recent survey and benchmark papers [42], [43] for more details.

C. Specific Region Segmentation

Specific Region Segmentation (SRS) we defined here refers to segmenting the specific region such as shadow [44]–[47], water [48], opacity [49], mirror [5], [50], and transparency [2]–[4], [51], [52] in the scene. Such regions are special and have a critical impact on the vision systems. For the shadow, water, opacity, and mirror region, there typically exists intensity or content discontinuities between the target region and background. Instead, both the intensity and content are typically similar between the glass region and the background, leading to a great challenge of glass segmentation. Transparency segmentation methods [3], [4], [52] consider both stuff such as window, door, and guardrail and things such as cup and eyeglass. We follow [2], [51] in this paper to focus on the segmentation of stuff (*i.e.*, relatively large glass region that brings great challenges to vision systems), studying the method that is exclusively about grouping glass but not about distinguishing between stuff and things.

D. Deep Feature Fusion

Deep Feature Fusion plays an important role in achieving high performance for many computer vision tasks. The common practice of fusing level-different features is to first upsample higher-level features via interpolation or transposed convolution and then perform channel-wise concatenation [23], [24], [37], [53]–[57] or element-wise addition [58], [59] between upsampled higher-level features and current-level features (Figure 2 (a)). Some methods [2], [5], [34], [60] adopt the attention mechanism in the fusion process, *i.e.*, using the attention map generated from the higher-level

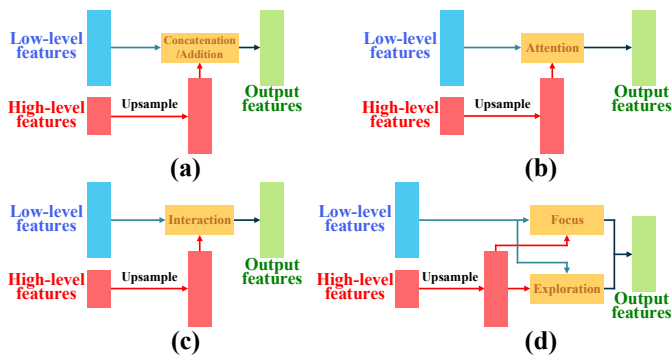


Fig. 2. Different strategies for fusing level-different features. (a) Fusion strategies of channel-wise concatenations or element-wise additions. (b) Fusion strategies use the attention map generated from the higher-level features to guide the current-level features. (c) Fusion strategies of mutual refinement or interaction. (d) Fusion strategies by simultaneously highlighting the common and exploring the difference between level-different features.

features to guide the current-level features (Figure 2 (b)). The strategies of mutual refinement [31] or interaction [26] are also developed (Figure 2 (c)). Our method differs from the above fusion strategies by simultaneously highlighting the common and exploring the difference between level-different features (Figure 2 (d)). And we validate the effectiveness of such design by the experiments.

III. METHODOLOGY

A. Motivation

To identify the existence of glass, human beings typically first *explore* and then *combine* different useful information including both low-level cues (*e.g.*, color difference between inside and outside the glass, blur/bright spot/ghost caused by reflection) and high-level contexts (*e.g.*, semantic relations between different objects). Existing glass segmentation methods make the attempt to explore useful cues from different levels of features in the deep network via large-field contextual feature extraction [2], boundary attention [3], or global relation modeling implemented by transformer [4]. However, how to effectively combine the obtained cues/features has rarely been focused and studied in the glass segmentation field. As different cues/features typically vary in level and characteristic, designing a reasonable fusion strategy rather than fusing them naively would naturally benefit more for the accurate glass segmentation.

Based on such observation, we focus in this paper on the effective feature fusion towards accurate glass segmentation. To this end, we first develop a novel level-different features fusion strategy which first uses a discriminability enhancement (DE) module (Sec. III-C) to bridge the characteristic gap between different levels of features and then fuses the enhanced features via a simple yet design-intuitive focus-and-exploration based fusion (FEBF) module (Sec. III-D). We then construct a progressive glass segmentation network (PGSNet) (Sec. III-B) by embedding our fusion strategy into an encoder-decoder framework, implementing a coarse-to-fine glass segmentation.

B. Overview

Figure 3 shows the overview of our proposed progressive glass segmentation network (PGSNet). Given a single RGB image, we first feed it into a ResNeXt-101 [61] backbone to extract multi-level features which are then fed into four discriminability enhancement (DE) modules to learn more discriminative feature representations for bridging the characteristic gap between level-different features. Second, we leverage the well-designed focus-and-exploration based fusion (FEBF) module to progressively aggregate level-adjacent features from high-level to low-level. Third, we apply a convolution layer with 3×3 kernel on the features generated from each of three FEBF modules to predict different levels of the glass segmentation map. Finally, we upsample the prediction map with the largest spatial size to obtain the original image resolution as the output.

C. Discriminability Enhancement Module

Different levels of features typically vary in characteristic. High-level features usually embed more semantic knowledge and contextual relations while low-level features have larger spatial sizes and keep richer and more detailed information such as edges, lines, and corners. The DE module is designed to bridge the characteristic gap by enhancing the discriminability for both high-level and low-level features before fusing them together.

Neuroscience experiments have verified that a set of various sized population receptive fields in the human visual system helps to highlight the area close to the retinal fovea, which is sensitive to small spatial shifts [62]. This motivates us to use multi-field processing to enhance the discriminability of high-level features for more precise target object location. On the other hand, it has been pointed out in [63] that the contexts in a large receptive field could help to enhance the semantics of low-level features, and thus could benefit the suppression of noise and redundant features. These two aspects of analysis inspire us to design the DE module which is applicable for both high-level and low-level features into a multi-branch structure, in which each branch captures different scales of large-field contexts.

Figure 4 illustrates the detailed structure of the discriminability enhancement (DE) module. Given the input level-specific features, the DM module aims to purify the features to be the more discriminative representations. Specifically, DE module consists of four parallel DE branches to perform the multi-field processing and the outputs of these four branches are combined to generate the output of the DE module. In each DE branch, the processing can be divided into three steps: local feature extraction (LFE), local feature fusion (LFF), and contextual feature perception (CFP). First, we apply a convolution layer with a kernel size of $k = 3$ for channel reduction and use two parallel $\{1 \times k, k \times 1\}$ and $\{k \times 1, 1 \times k\}$ spatially separable convolutions with the dilation rate of r to efficiently capture the local region information. Practically, for the spatially separable convolutions in four DE branches, the kernel size k is set to 3, 5, 7, 9, and the dilation rate r is set to 1, 2, 3, 4, respectively. Second, we concatenate the local

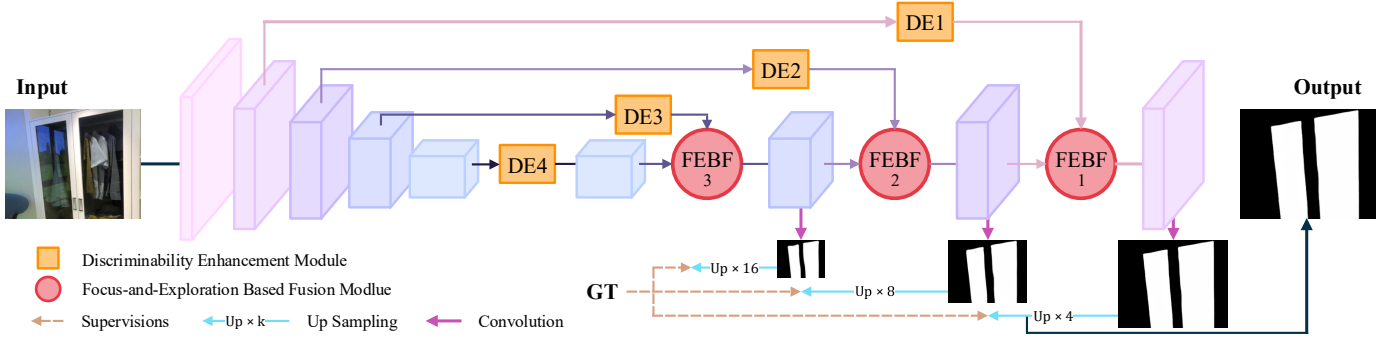


Fig. 3. The architecture of our proposed progressive glass segmentation network (PGSNet).

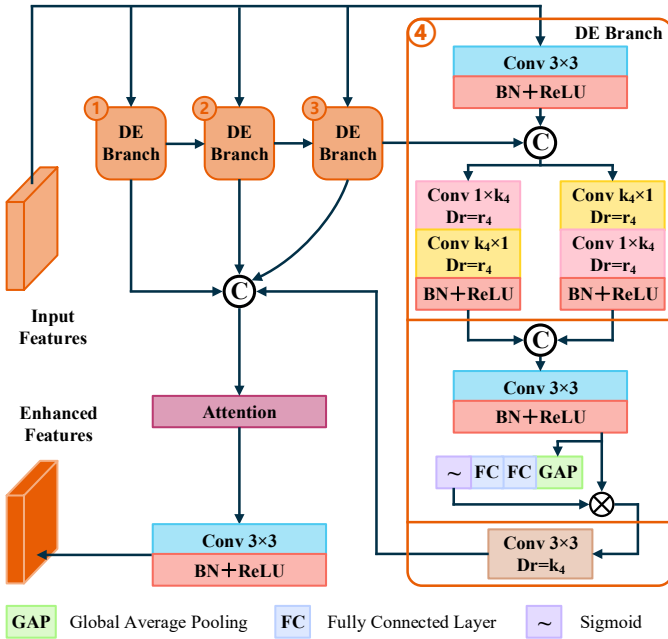


Fig. 4. Detailed illustration of our proposed discriminability enhancement (DE) module.

features in channel and apply a 3×3 convolution followed by the channel recalibration [64] for local feature fusion. Third, we employ a 3×3 convolution with a dilation rate of $r = k$ to perceive contextual information in a large receptive field. Following [2], we also add information flow between adjacent branches to facilitate the feature extraction in a larger field-of-view.

D. Focus-and-Exploration Based Fusion Module

Aggregating different levels of features usually introduces ambiguous features or leads to loss of details, which both make the network fail to optimize. The focus-and-exploration based fusion (FEBF) module is designed to alleviate these two cases via highlighting the common (focus) and exploring the difference (exploration) between level-different features, respectively.

As depicted in Figure 5, the FEBF module takes two level-different features as input and outputs the fused fea-

tures. Specifically, given the input high-level features $F_h \in \mathbb{R}^{C_h \times H_h \times W_h}$ and low-level features $F_l \in \mathbb{R}^{C_l \times H_l \times W_l}$, where $C_{h/l}$, $H_{h/l}$, and $W_{h/l}$ represent the channel number, height, and width, respectively, we first do the following to make them keep the same in spatial size and channel:

$$F'_h = \mathcal{R}(\mathcal{N}(\psi_{3 \times 3}(\mathcal{U}(F_h))))), \quad (1)$$

$$F'_l = \mathcal{R}(\mathcal{N}(\psi_{3 \times 3}(F_l))), \quad (2)$$

where $\psi_{3 \times 3}$ is a convolution layer with a kernel size of 3; \mathcal{U} is the bilinear upsampling; \mathcal{N} is the batch normalization (BN); and \mathcal{R} is the ReLU activation function. Then, we highlight the common and explore the difference between F'_h and F'_l in the focus and exploration branch, respectively.

$$F_f = \mathcal{R}(\mathcal{N}(\psi_{3 \times 3}(\mathcal{R}(\mathcal{N}(\psi_{3 \times 3}((F'_l \otimes F'_h) \oplus F'_l))) \oplus \mathcal{R}(\mathcal{N}(\psi_{3 \times 3}((F'_l \otimes F'_h) \oplus F'_h)))))), \quad (3)$$

$$F_e = \mathcal{R}(\mathcal{N}(\psi_{3 \times 3}(F'_l \ominus F'_h))), \quad (4)$$

where \otimes , \oplus , and \ominus denote the element-wise multiplication, addition, and subtraction, respectively. Finally, we can obtain the output features $F_o \in \mathbb{R}^{C_l \times H_l \times W_l}$ by:

$$F_o = \mathcal{R}(\mathcal{N}(\psi_{3 \times 3}(\alpha F_f \oplus \beta F_e))), \quad (5)$$

where α and β are the learnable scale parameters which are initialized as 1.

Note that the subtraction operation used in our FEBF module differs from [65] and [66] in both motivation and implementation. Ding *et al.* [65] conduct the subtraction between the local and contextual features to perceive the contextual contrasted features for locating discriminative objects. Li *et al.* [66] perform the subtraction between segmentation features and body features to harvest edge features which are supervised by ground truth edge map for explicitly modeling the different parts of objects. Our motivation to use subtraction operation between different features is to screen out the uncertain areas for further supporting the effective fusion strategy. Different levels of features typically generate different responses related to the glass. For example, high-level features tend to be activated on the coarse location of the glass region while low-level features usually have a high response on the detailed boundaries. The regions with high values in both high-level and low-level features are more likely to belong to the glass region. Thus we use *addition* operation to make

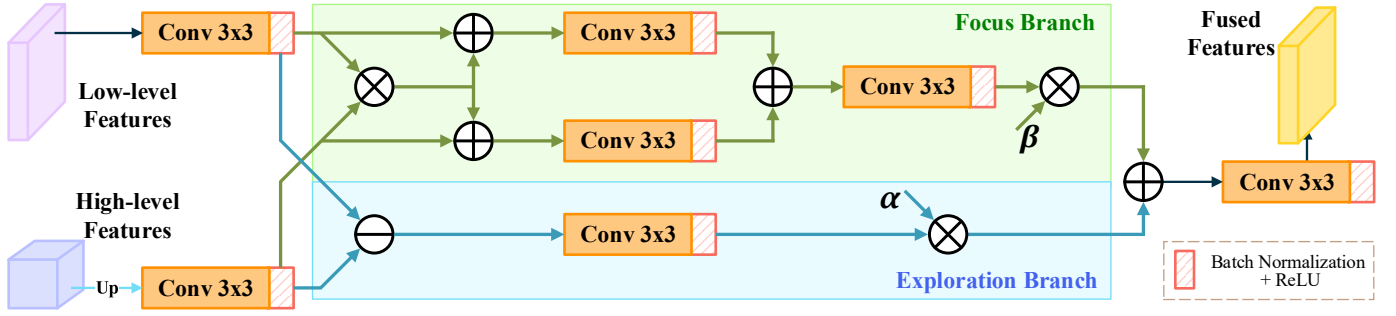


Fig. 5. Detailed illustration of our proposed focus-and-exploration based fusion (FEBF) module.

the network *focus* on such regions. For the regions with high responses in one features while have low values in another one features are the uncertain areas. We adopt the *subtraction* operation to screen out such regions and then use a convolution layer to further *explore* the true glass regions. Finally, the *focus* features and *exploration* features are combined, generating more precise features for glass segmentation.

E. Loss Function

We train our PGSNet with a hybrid loss defined as:

$$\mathcal{L}_{\text{hybrid}} = \gamma \mathcal{L}_{\text{bce}} + \lambda \mathcal{L}_{\text{iou}}, \quad (6)$$

where \mathcal{L}_{bce} and \mathcal{L}_{iou} denote the binary cross-entropy (BCE) loss [67] and IoU loss [68], respectively. γ and λ are the balancing parameters and we empirically set them to 1. BCE loss [67] is the most widely used loss in binary classification and segmentation tasks, which calculates the loss for each pixel independently. It is a pixel-wise measure which helps with the convergence on all pixels. As BCE loss [67] weights both the foreground and background pixels equally, the loss of foreground pixels will be diluted for images where the background is dominant. Hence, we further include the map-level IoU loss [68] which could make the network focus more on the foreground regions and output the complete segmentation results. To facilitate the learning process, we adopt the deep supervision [69]. The overall loss function is:

$$\mathcal{L}_{\text{overall}} = \sum_{i=1}^3 2^{(3-i)} \mathcal{L}_{\text{hybrid}}^i, \quad (7)$$

where $\mathcal{L}_{\text{hybrid}}^i$ denotes the hybrid loss between the ground truth glass mask and the prediction from the fused features generated by the FEBF module at the i -th level.

IV. EXPERIMENTS

A. Dataset

We evaluate the effectiveness of our method on two benchmark datasets GDD [2] and Trans10K-Stuff [3] as well as our newly constructed home-scene-oriented (HSO) glass segmentation dataset. GDD [2] is the first glass segmentation dataset in the deep learning era, which consists of 2,980 training images and 936 testing images. Trans10K [3] is a large-scale transparent object segmentation dataset, containing two categories of objects, *i.e.*, stuff and things. As the

TABLE I
COMPOSITION OF OUR HSO DATASET.

Dataset	Images	Train	Test
Matterport3D [70]	4,451	2,887	1,564
2D3DS [73]	295	162	133
ScanNet [72]	68	17	51
SUNRGBD [71]	38	4	34
Total	4,852	3,070	1,782

glass segmentation task we strive to address is exclusively about grouping but not about identifying object categories, we only use the “stuff” images and corresponding annotations in Trans10K [3]. In our experiment, 2,455 glass image/mask pairs in Trans10K-Stuff [3] are used for training and 1,771 images in both validation and testing set are used for testing.

Our HSO dataset is built to further diversify the patterns of glass, especially the glass in home scenes, for advancing household robot applications and in-depth research on this topic. Instead of capturing the glass images ourselves, we compose the HSO dataset from selected exemplars from four popular datasets (*i.e.*, Matterport3D [70], SUNRGBD [71], ScanNet [72], and 2D3DS [73]) to ensure a wide diversity and broad coverage. See Table I for a summary and Figure 6 for representative examples. Each selected image contains at least one glass region, and the pixel-level accurate reference glass masks are created by professional annotators. The statistics of HSO dataset are shown in Figure 7, where we can see that HSO has glass with reasonable property distributions in terms of location, area, scene, and global color contrast. We will release HSO to stimulate further research on this topic.

B. Experimental Setup

1) *Evaluation Metrics*: For a comprehensive evaluation, we adopt four widely used metrics for quantitatively assessing the mirror segmentation performance: intersection over union (IoU), weighted F-measure (F_{β}^w) [74], mean absolute error (MAE), and balance error rate (BER) [75].

The intersection over union (IoU) is widely used in the segmentation field, which is defined as:

$$IoU = \frac{\sum_{i=1}^H \sum_{j=1}^W (G(i, j) * P_b(i, j))}{\sum_{i=1}^H \sum_{j=1}^W (G(i, j) + P_b(i, j) - G(i, j) * P_b(i, j))}, \quad (8)$$

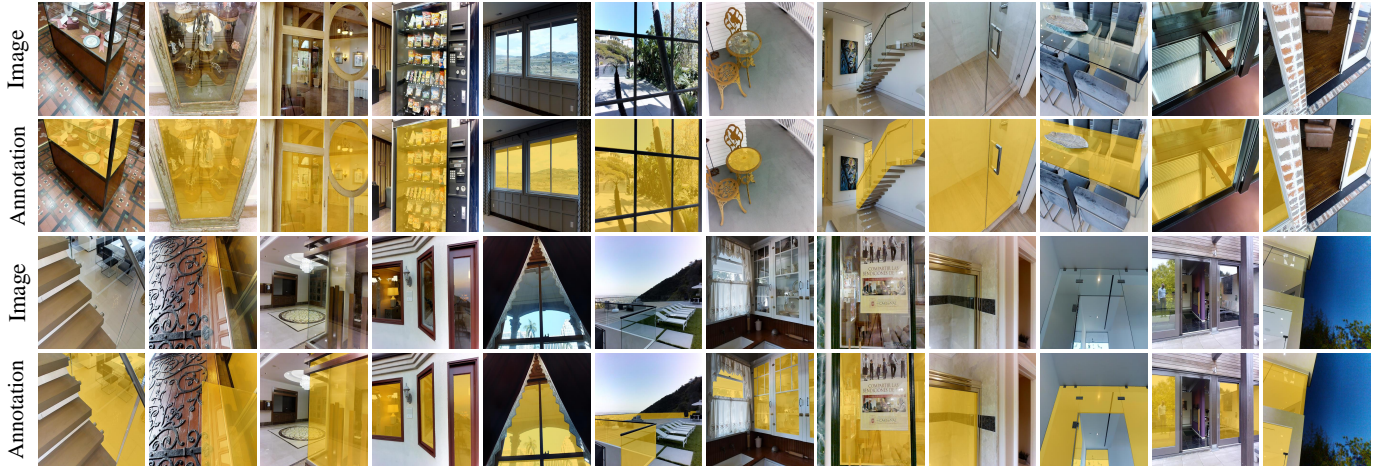


Fig. 6. Example glass image/mask pairs in our HSO dataset. It shows that HSO covers diverse types of glass in various home scenes.

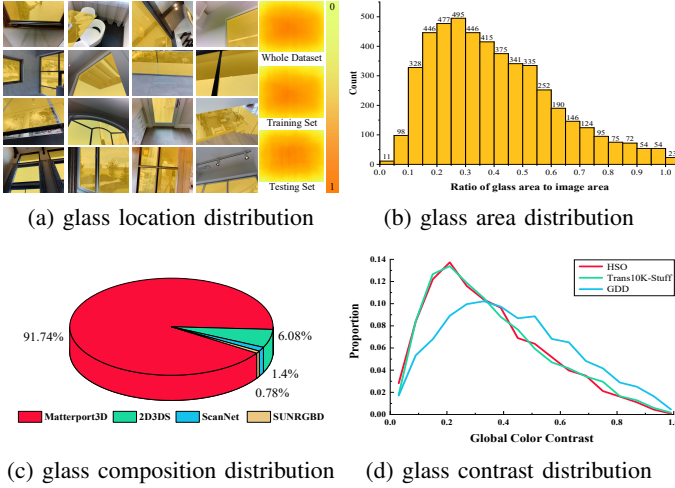


Fig. 7. Statistics of our HSO dataset.

where G is the ground truth mask in which the values of the glass region are 1 while those of the non-glass region are 0; P_b is the predicted mask binarized with a threshold of 0.5; and H and W are the height and width of the ground truth mask, respectively.

We also adopt the weighted F-measure metric from the salient object detection field. F-measure (F_β) is a comprehensive measure on both the precision and recall of the prediction map. Recent studies [76], [77] have suggested that the weighted F-measure (F_β^w) [74] can provide more reliable evaluation results than the traditional F_β . Thus, we report F_β^w in the comparison.

The mean absolute error (MAE) metric is widely used in foreground-background segmentation tasks, which calculates the element-wise difference between the prediction map P and the ground truth mask G :

$$MAE = \frac{1}{H \times W} \sum_{i=1}^H \sum_{j=1}^W |P(i, j) - G(i, j)|, \quad (9)$$

where $P(i, j)$ indicates the predicted probability score at

location (i, j) .

The last metric is the balance error rate (BER), which is a standard metric in the shadow detection field, defined as:

$$BER = \left(1 - \frac{1}{2} \left(\frac{TP}{N_p} + \frac{TN}{N_n}\right)\right) \times 100, \quad (10)$$

where TP , TN , N_p , and N_n represent the numbers of true positive pixels, true negative pixels, glass pixels, and non-glass pixels, respectively.

Note that for IoU and F_β^w , it is the higher the better, while for MAE and BER , it is the lower the better.

2) *Implementation Details*: We implement our model with the PyTorch toolbox [78]. We train and test our model on a PC with an Intel Core i7-7700K 4.2GHz CPU (with 32GB RAM) and an NVIDIA Titan V GPU (with 12GB memory). The strategies of training and testing on three datasets keep the same. Specifically, for training, input images are augmented by randomly horizontal flipping and resizing. The parameters of the backbone network are initialized with the ResNeXt-101 model [61] pre-trained on ImageNet [79] while the remaining layers of our model are initialized randomly. We use the stochastic gradient descent (SGD) optimizer with the momentum of 0.9 and the weight decay of 5×10^{-4} for loss optimization. We set the batch size to 6 and adjust the learning rate by the poly strategy [80] with the basic learning rate of 0.001 and the power of 0.9. It takes about 14, 16, and 21 hours for the network to converge after 170, 220, and 250 epochs for the training on GDD [2], Trans10K-Stuff [3], and our HSO dataset, respectively. For testing, the image is first resized to 352×352 for network inference and then the output map is resized back to the original size of the input image. Both the resizing processes use bilinear interpolation. We do not use any post-processing such as the fully connected conditional random field (CRF) [81] to further enhance the final output. The inference for a 352×352 image takes only 0.047 seconds (about 21 FPS).

3) *Compared Methods*: We validate the effectiveness of our method by comparing it with 26 methods selected from other related fields according to the following criteria: (i) classical

TABLE II

QUANTITATIVE COMPARISON TO THE STATE-OF-THE-ART METHODS ON THE GDD [2], TRANS10K-STUFF [3] AND OUR NEWLY CONSTRUCTED HSO DATASET. ALL THE METHODS ARE RE-TRAINED ON THE CORRESPONDING TRAINING SET. † DENOTES USING CRFS [81] FOR POST-PROCESSING. "STATISTICS" MEANS THRESHOLDING GLASS LOCATION STATISTICS FROM THE CORRESPONDING TRAINING SET AS A GLASS MASK FOR SEGMENTATION. •: SEMANTIC SEGMENTATION METHOD. ◦: SALIENT OBJECT DETECTION METHOD. Δ: SHADOW DETECTION METHODS. §: MEDICAL IMAGE SEGMENTATION METHOD. *: MIRROR SEGMENTATION METHOD. ◊: TRANSPARENT OBJECT SEGMENTATION. ✱: GLASS SEGMENTATION METHODS. THE FIRST, SECOND, AND THIRD BEST RESULTS ARE MARKED IN RED, GREEN, AND BLUE, RESPECTIVELY. OUR METHOD ACHIEVES THE BEST PERFORMANCE ON ALL THREE CHALLENGING DATASETS UNDER FOUR STANDARD METRICS.

Methods	Pub.'Year	Backbone	GDD [2]				Trans10K-Stuff [3]				HSO (Ours)			
			Trainset:2,980		Testset:936		Trainset:2,455		Testset:1,771		Trainset:3,070		Testset:1,782	
			IoU↑	F_{β}^w ↑	MAE↓	BER↓	IoU↑	F_{β}^w ↑	MAE↓	BER↓	IoU↑	F_{β}^w ↑	MAE↓	BER↓
Statistics	-	-	40.75	0.427	0.451	39.31	45.88	0.448	0.371	27.28	28.86	0.311	0.485	44.84
ICNet• [82]	ECCV'18	ResNet-50	69.59	0.747	0.164	16.10	74.94	0.784	0.110	10.92	62.15	0.674	0.165	17.07
PSPNet• [14]	CVPR'17	ResNet-50	84.06	0.867	0.084	8.79	87.89	0.907	0.045	5.46	77.60	0.814	0.095	10.57
DeepLabv3+• [83]	ECCV'18	ResNet-50	69.95	0.767	0.147	15.49	51.52	0.602	0.229	23.80	64.47	0.705	0.149	16.03
DenseASPP• [11]	CVPR'18	ResNet-50	83.68	0.867	0.081	8.66	86.34	0.894	0.051	6.12	75.94	0.805	0.096	11.34
BiSeNet• [12]	ECCV'18	ResNet-50	80.00	0.830	0.106	11.04	85.82	0.885	0.056	6.11	75.85	0.798	0.101	11.04
DANet• [9]	CVPR'19	ResNet-50	84.15	0.864	0.089	8.96	88.18	0.907	0.045	5.28	77.69	0.817	0.091	10.60
CCNet• [10]	ICCV'19	ResNet-50	84.29	0.867	0.085	8.63	88.20	0.906	0.044	5.15	78.17	0.820	0.092	10.34
GFFNet• [17]	AAAI'20	ResNet-50	82.41	0.855	0.090	9.11	69.29	0.747	0.143	14.19	77.34	0.810	0.094	9.69
SFNet• [16]	ECCV'20	ResNet-50	80.96	0.848	0.102	10.23	71.27	0.767	0.133	13.14	77.48	0.814	0.091	10.79
FaPN• [18]	ICCV'21	ResNet-101	86.65	0.887	0.062	5.69	89.09	0.913	0.042	4.80	78.05	0.835	0.089	9.51
DSS◦ [23]	TPAMI'19	ResNet-50	80.24	0.799	0.123	9.73	84.77	0.855	0.075	6.42	73.08	0.730	0.135	12.04
PiCANet◦ [32]	CVPR'18	ResNet-50	83.74	0.848	0.093	8.24	83.99	0.843	0.077	7.03	71.66	0.730	0.148	13.31
RAS◦ [33]	ECCV'18	ResNet-50	80.96	0.830	0.106	9.48	85.40	0.882	0.062	6.20	74.63	0.775	0.116	11.24
CPD◦ [34]	CVPR'19	ResNet-50	82.52	0.850	0.095	8.87	86.08	0.869	0.064	5.89	76.16	0.789	0.111	10.58
EGNet◦ [39]	ICCV'19	ResNet-50	85.05	0.870	0.083	7.43	84.57	0.863	0.068	6.59	74.29	0.771	0.119	11.58
F3Net◦ [31]	AAAI'20	ResNet-50	84.79	0.870	0.082	7.38	86.23	0.881	0.061	5.81	76.84	0.799	0.105	10.58
MINet-R◦ [26]	CVPR'20	ResNet-50	82.03	0.847	0.092	8.55	85.88	0.881	0.06	6.03	76.61	0.798	0.104	10.33
ITSD◦ [84]	CVPR'20	ResNet-50	83.72	0.862	0.087	7.77	85.44	0.871	0.063	6.26	74.33	0.776	0.123	11.39
DSCΔ [44]	CVPR'18	ResNet-50	83.56	0.855	0.090	7.97	86.37	0.882	0.058	5.65	74.79	0.773	0.119	11.14
BDRARΔ† [46]	ECCV'18	ResNet-50	80.01	0.847	0.098	9.87	85.00	0.870	0.061	6.04	75.32	0.802	0.101	11.13
PraNet§ [85]	MICCAI'20	ResNet-50	82.06	0.847	0.098	9.33	87.15	0.881	0.058	5.31	71.93	0.756	0.128	13.11
MirrorNet✱† [5]	ICCV'19	ResNeXt-101	85.07	0.866	0.083	7.67	88.30	0.907	0.047	4.95	78.82	0.820	0.102	9.93
TransLab◊ [3]	ECCV'20	ResNet-50	81.64	0.849	0.097	9.70	87.10	0.897	0.051	5.44	74.32	0.781	0.123	12.00
Trans2Seg◊ [4]	IJCAI'21	ResNet-50	84.41	0.872	0.078	7.36	74.98	0.767	0.124	10.73	77.98	0.817	0.095	9.65
GDNet✱ [2]	CVPR'20	ResNeXt-101	87.63	0.898	0.063	5.62	88.68	0.907	0.046	4.72	78.73	0.817	0.097	9.32
GSD✱ [51]	CVPR'21	ResNeXt-101	87.53	0.895	0.066	5.90	89.67	0.917	0.042	4.52	78.86	0.818	0.103	9.79
PGSNet✱	Ours	ResNeXt-101	87.81	0.901	0.062	5.56	89.79	0.917	0.042	4.39	80.06	0.836	0.089	9.08

TABLE III

COMPARISON BETWEEN OUR PGSNET AND STATE-OF-THE-ART GLASS SEGMENTATION METHODS ON THE GSD DATASET [51].

Methods	Pub.'Year	Backbone	GSD [51]			
			IoU↑	F_{β}^w ↑	MAE↓	BER↓
TransLab [3]	ECCV'20	ResNet-50	78.05	0.828	0.069	9.19
Trans2Seg [4]	IJCAI'21	ResNet-50	79.65	0.839	0.069	8.21
GDNet [2]	CVPR'20	ResNeXt-101	82.51	0.857	0.058	6.41
GSD [51]	CVPR'21	ResNeXt-101	83.64	0.903	0.055	6.12
PGSNet	Ours	ResNeXt-101	83.65	0.868	0.054	6.25

architectures, (ii) recently published, and (iii) achieving state-of-the-art performance in the specific field. Specifically, we choose semantic segmentation methods ICNet [82], PSPNet [14], DeepLabv3+ [8], DenseASPP [11], BiSeNet [12], DANet [9], CCNet [10], GFFNet [17], SFNet [16] and FaPN [18]; salient object detection methods DSS [23], PiCANet [32], RAS [33], CPD [34], EGNet [39], F3Net [31], MINet-R [26], and ITSD [84]; shadow detection methods DSC [44] and BDRAR [46]; medical image segmentation method PraNet [85]; mirror segmentation method MirrorNet [5]; transparent object segmentation methods TransLab [3] and Trans2Seg [4];

and glass segmentation method GDNet [2] and GSD [51]. For a fair comparison, we use either their publicly available codes or the implementations with recommended parameter settings. For each of the three datasets, all the models are retrained on the corresponding training set. Besides, all the prediction maps are evaluated with the same code.

C. Comparison with the State-of-the-arts

Table II reports the quantitative results of our method against other 26 state-of-the-art methods on two benchmark datasets and our newly constructed HSO dataset. We can see that our method outperforms all the other methods on all three challenging datasets under all four standard metrics. Notably, compared with the state-of-the-art glass segmentation method GDNet [2], our method improves IoU and F_{β}^w by 1.33% and 1.90% on the HSO dataset, respectively. Noteworthy is that our HSO dataset leads to a ~10% IoU drop for all methods in Table II, reflecting the large room to achieve accurate glass segmentation and the necessity of the new HSO dataset for stimulating further research. We also retrained our PGSNet on the GSD dataset [51] and presented the results in Table III. It can be seen that our PGSNet achieves comparable performance

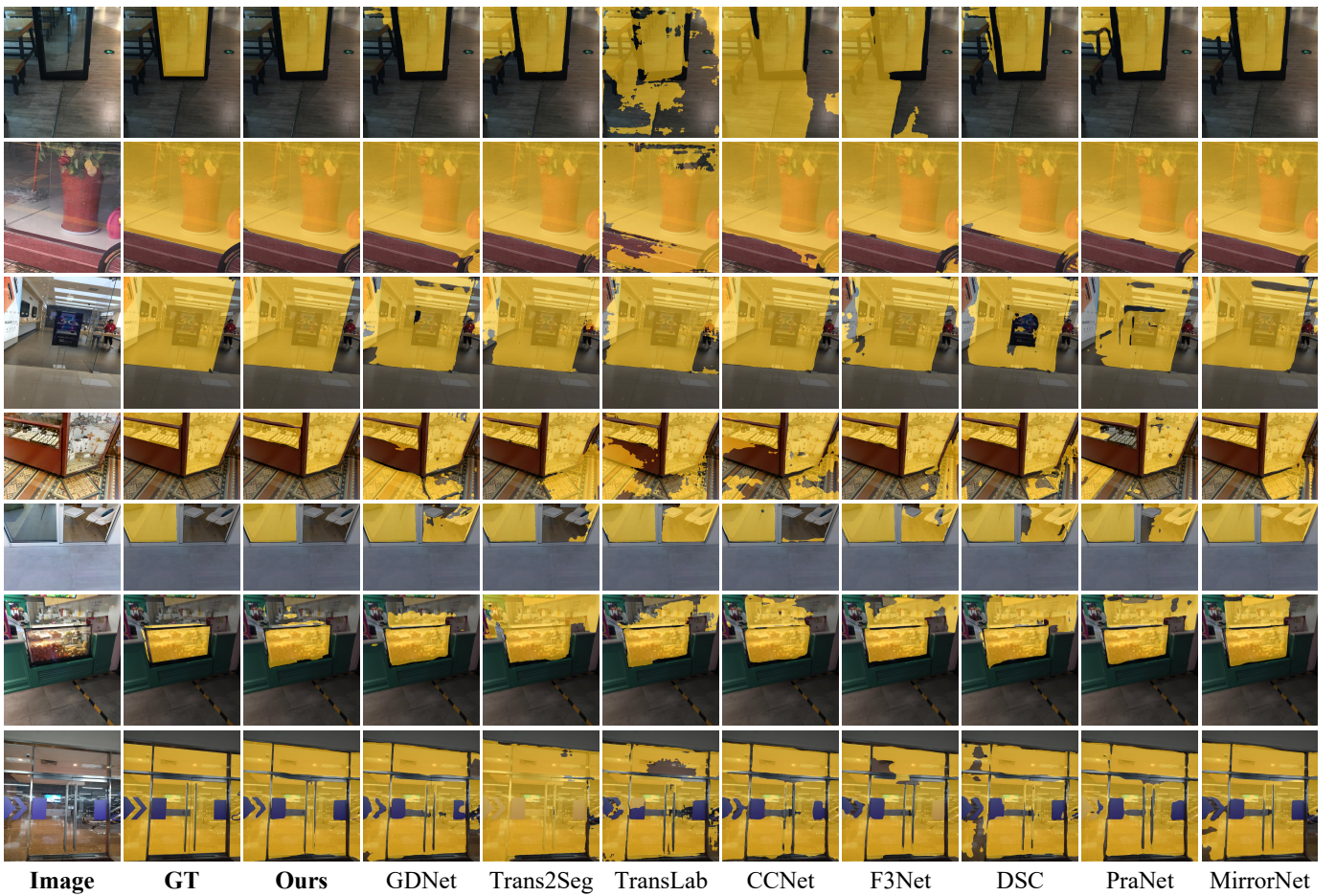


Fig. 8. Visual comparison of the proposed model with state-of-the-art methods. Obviously, our approach is capable of segmenting glass in various scenes more accurately.

against state-of-the-arts. Besides, Figure 8 qualitatively compares our PGSNet with three prior glass/transparency segmentation methods (*i.e.*, GDNNet [2], Trans2Seg [3], and TransLab [3]) as well as the best approach from each of the six other categories (*i.e.*, semantic segmentation method CCNet [10], salient object detection method F3Net [31], shadow detection method DSC [44], medical image segmentation method PraNet [85], and mirror segmentation method MirrorNet [5]). It can be seen that our method is capable of accurately segmenting small glass regions (*e.g.*, 1st row), large glass regions (*e.g.*, 2-nd and 3-rd rows), and multiple glass regions (*e.g.*, 4-th row). This is mainly because that the discriminability enhancement (DE) module can explore different scales of contexts and purify the features to be the more discriminative representations, benefiting the more accurate positioning of glass regions. While the state-of-the-arts are typically confused by the background which shares similar appearance with the glass regions (*e.g.*, 5-th row) or the glass region that cluttered in the background (*e.g.*, 6-th row), our method can successfully infer the true glass region. This is mainly contributed by the proposed focus-and-exploration based fusion (FEBF) module which could help eliminate the ambiguous features and augment the details. Furthermore, benefited by the progressive features fusion from high-level to low-level, our method can effectively perceive the detailed information and thus has the ability to finely segment the glass regions with complex structures (*e.g.*, the last row).

D. Ablation Study

Our work is motivated by the fact that existing glass segmentation methods ignore the importance of the effective fusion of different features/cues. We design the DE module as a multi-/large-field processing paradigm based on the observation that a set of various sized population receptive fields helps to perceive the small spatial shifts and the contexts in a large receptive field could help to enhance the features semantic. The FEBF module is designed to alleviate both the introduction of ambiguous and loss of details in the fusion via highlighting the common and exploring the difference between level-different features, respectively.

In this subsection, we conduct ablation studies to validate the effectiveness of two key components tailored for effective features fusion towards accurate glass segmentation, *i.e.*, discriminability enhancement (DE) module and focus-and-exploration based fusion (FEBF) module, as well as explore the impact of different feature extractors, and report the experimental results in Table IV, V, VI, and Figure 9.

1) *The effectiveness of DE module*: We first define and train a base model “B” (*i.e.*, A in Table IV) which is based on PGSNet but the feature fusion strategy (*i.e.*, DE module and FEBF module) is replaced by the concatenation fusion strategy. Starting from the base model, we gradually re-introduce the LFE, LFF, and CFP in the DE module (B-D). From the results, we observe that: (i) DE module can



Fig. 9. Visual examples that reveal the rationality behind the FEBF module design. It visualizes both input low-level features (the 3rd column) and high-level features (the 4th column) as well as output features (the last column) of the FEBF module, together with the intermediate features passed through the focus branch (the 5th column) and exploration branch (the 6th column) in the FEBF module. Although the input low-level features are full of noise and the input high-level features are coarse, the focus branch can highlight the common and the exploration branch can explore the difference, making the final output features of the FEBF module more discriminative.

TABLE IV

QUANTITATIVE ABLATION RESULTS THAT INDICATE THAT EACH COMPONENT IN PGSNET CONTRIBUTES TO THE OVERALL PERFORMANCE.

“B” DENOTES OUR NETWORK WITH OUR PROPOSED FEATURE FUSION STRATEGY (*i.e.*, DISCRIMINABILITY ENHANCEMENT (DE) MODULE AND FOCUS-AND-EXPLORATION BASED FUSION (FEBF) MODULE) REPLACED BY THE CONCATENATION FUSION STRATEGY. “LFE”, “LFF”, AND “CFP” ARE THE LOCAL FEATURE EXTRACTION, LOCAL FEATURE FUSION, AND CONTEXTUAL FEATURE PERCEPTION IN DE MODULE, RESPECTIVELY.

Networks		GDD [2]			
		IoU \uparrow	$F_{\beta}^w\uparrow$	MAE \downarrow	BER \downarrow
A	B (<i>i.e.</i> , Concatenation Fusion)	85.63	0.881	0.075	7.04
B	B + DE w/ LFE only	87.28	0.893	0.066	6.01
C	B + DE w/ LFE&LFF only	87.57	0.896	0.065	5.94
D	B + DE w/ LFE&LFF&CFP	87.61	0.897	0.063	5.75
E	B w/ Addition Fusion	86.02	0.885	0.071	6.84
F	B w/ Multiplication Fusion	85.88	0.885	0.073	6.90
G	B + FEBF w/ Focus only	86.22	0.888	0.070	6.72
H	B + FEBF w/ Focus&Exploration	86.55	0.888	0.071	6.56
I	B + DE + FEBF (<i>i.e.</i> , PGSNet)	87.81	0.901	0.062	5.56

help boost the segmentation performance largely (*i.e.*, *D* is better than *A*) as the DE bridges the characteristic gap between level-different features and thus benefit the effective features fusion; (ii) applying multi-field processing on the level-specific features before fusing them together is helpful (*i.e.*, *B* is better than *A*), indicating that multi-field processing is essential for making features more discriminative and more suitable for fusion; (iii) channel recalibration [64] can help integrate local features (*i.e.*, *C* is better than *B*); and (iv) perceiving contextual information can further improve the segmentation performance (*i.e.*, *D* is better than *C*). Note that as a pre-step in features fusion, DE module does NOT aim to explore specific glass-related cues but to enhance the features discriminability for effective features fusion. It differs from the LCFI module [2] in that it has the *extra* local feature fusion (LFF) and contextual feature perception (CFP) which can effectively aggregate local features and enlarge the receptive field, respectively. The ablation study results (*i.e.*, *B-D* in Table IV) validate the effectiveness of these two components. Besides, the experimental results in Table V further demonstrate the superiority of our proposed DE module over general attention modules (*i.e.*, channel attention, spatial attention, and combination of the two).

2) *The effectiveness of FEBF module*: Compared to the concatenation fusion strategy (*i.e.*, *A* in Table IV), the strategies of addition (*E*) and multiplication (*F*) fusion (as shown in Figure 2 (a)) perform similarly. Due to characteristic gap between level-different features and redundant information in the fusion results, these simple fusion strategies would limit

TABLE V

QUANTITATIVE ABLATION RESULTS THAT DEMONSTRATE THE SUPERIORITY OF OUR PROPOSED DE MODULE OVER GENERAL ATTENTION MODULES (*i.e.*, CHANNEL ATTENTION, SPATIAL ATTENTION, AND COMBINATION OF THE TWO).

Networks	GDD [2]			
	IoU \uparrow	$F_{\beta}^w\uparrow$	MAE \downarrow	BER \downarrow
PGSNet w/o attention	86.55	0.888	0.071	6.56
PGSNet w/ channel attention	86.60	0.892	0.066	6.51
PGSNet w/ spatial attention	86.98	0.893	0.068	6.30
PGSNet w/ channel+spatial attention	87.22	0.892	0.068	6.18
PGSNet w/ DE module	87.81	0.901	0.062	5.56

the accuracy of glass segmentation tasks. By highlighting the common between level-different features in the fusion process (*i.e.*, *G*, also shown in Figure 2 (c)), a better performance can be achieved. When further introduce the exploration of features difference (*i.e.*, *H*, also shown in Figure 2 (d)), we get improved results. Also shown in the fourth to seventh rows in Figure 8, when the glass regions are in similar patterns/semantic information with surroundings or have strong reflections, our FEBF module is superior to the traditional attention or interaction mechanism. This clearly demonstrates that our FEBF is more effective for features fusion towards accurate glass segmentation. Finally, the combination of DE and FEBF module (*i.e.*, *I*) enables our approach to possess the strong capability of accurately segmenting the glass.

We further visualize both input and output features of FEBF module in Figure 9 to validate the rationality behind the module design. As we can see, the input low-level features are full of noise (the 3rd column) and the input high-level features are coarse (inaccurate for the glass boundary region, the 4th column). The focus branch in FEBF module can highlight the common (the 5th column) and the exploration branch can explore the difference (the 6th column) between low-level and high-level features, respectively. And the combination of features from both focus branch and exploration branch gets more pure and accurate glass features (the last column). In conclusion, our well-designed FEBF module can effectively alleviate the introduction of ambiguous features and the loss of details when aggregating different levels of features, and thus can facilitate the optimization of the whole network.

3) *The impact of different feature extractors*: We follow [2] to use ResNeXt-101 [61] as the backbone to extract different levels of features. We further investigate the performance of more shallow/lightweight feature extractors and report the results in Table VI. We can observe that using more simple feature extractors (*i.e.*, VGG-16 [86] or ResNet-50 [87]) will

TABLE VI
COMPARISON BETWEEN OUR PGSNET AND OTHER SOTA METHODS UNDER DIFFERENT FEATURE EXTRACTORS.

Methods	Pub.'Year	Backbone	GDD [2]			
			IoU \uparrow	$F_{\beta}^w\uparrow$	MAE \downarrow	BER \downarrow
TransLab [3]	ECCV'20	ResNet-50	81.64	0.849	0.097	9.70
Trans2Seg [4]	IJCAI'21	ResNet-50	84.41	0.872	0.097	7.36
GNet [2]	CVPR'20	ResNet-50	85.23	0.877	0.074	6.65
PGSNet	Ours	VGG-16	86.92	0.891	0.067	6.20
PGSNet	Ours	ResNet-50	86.88	0.890	0.067	6.00
PGSNet	Ours	ResNeXt-101	87.81	0.901	0.062	5.56

lead to the performance decline in some extent. However, our PGSNet still achieve better results than other SOTA methods under the same simple feature extractors, showing the superiority of our method over the others.

E. Computational Cost

We show the computational efficiency comparison between our PGSNet and state-of-the-art glass segmentation methods GNet [2] and GSD [51] in Table VII. Under each input resolution, our PGSNet needs less than half of the FLOPs compared to GNet [2] and slightly higher FLOPs than GSD [51]. Note that GNet [2], GSD [51], and our PGSNet achieve the best performance with the input scale of 416, 384, and 352, respectively, which means that our PGSNet is more efficient than the other two methods (*i.e.*, 80.789 vs 271.533/92.697) while has superior segmentation performance (please refer to the quantitative comparison results shown in Table II).

TABLE VII
COMPARISON OF THE COMPUTATIONAL EFFICIENCY BETWEEN OUR PGSNET AND STATE-OF-THE-ART GLASS SEGMENTATION METHODS GNET [2] AND GSD [51]. * INDICATES THE RESOLUTION UNDER WHICH THE BEST PERFORMANCE IS ACHIEVED FOR EACH METHOD.

Methods	FLOPs (G)		
	Size: 352 \times 352	Size: 384 \times 384	Size: 416 \times 416
GNet [2]	191.411	231.365	271.533*
GSD [51]	77.892	92.697*	108.790
PGSNet	80.789*	96.145	112.837

F. Influence of receptive field

Glass segmentation is different from appearance-formulation-based semantic segmentation and it heavily relies on the context. Towards accurate glass segmentation, existing state-of-the-art methods explore the context in diverse manners. For example, GNet [2] harvests large-field contexts via a well-designed LCFI module, TransLab [3] and Trans2Seg [4] leverages non-local operations to perceive long-range contexts, and GSD [51] aggregates rich contexts with the RCAM module. In our work, we also explore the context by implementing a DE module. Our DE module is based on the LCFI module [2] but has two extra novel designs (*i.e.*, local feature fusion LFF and contextual feature perception CFP). The LFF and CFP help further enlarge the receptive field and their effectiveness has been validated by our experiments (Table IV). As it is hard to calculate the exact receptive field of existing complicated networks, we

TABLE VIII
QUANTITATIVE ABLATION RESULTS THAT REVEAL THE INFLUENCE OF RECEPTIVE FIELDS.

Networks	GDD [2]			
	IoU \uparrow	$F_{\beta}^w\uparrow$	MAE \downarrow	BER \downarrow
PGSNet w/ one DE branch	86.85	0.895	0.067	6.28
PGSNet w/ two DE branches	86.86	0.898	0.069	6.17
PGSNet w/ four DE branches	87.81	0.901	0.062	5.56

instead further explore the influence of the receptive field on glass segmentation by conducting experiments that vary the number of DE branches to achieve different receptive fields. From Table VIII, we can see that, despite possessing a larger receptive field, the PGSNet model with two DE branches performs similarly to the one with only one DE branch. We infer the reason behind this is that the performance of PGSNet is not tied to a single component but due to the interplay of all components combined. As such, PGSNet offers a holistic glass segmentation system that could cover the gap of small receptive field differences. When adopting four DE branches (*i.e.*, the full PGSNet model), the receptive field becomes much larger than the former two variants which brings performance improvement to some extent. These experiments show that the receptive field indeed has an influence on glass segmentation and presents a the larger the better trend in a certain range.

G. Loss function and training strategy

We use the same loss function as [2] to optimize or network the same multi-scale supervision training strategy from [31]. To verify the importance of the lesser-used IoU loss and the multi-scale training strategy, we compare our PGSNet with the ones without IoU loss for training and without multi-scale training strategy in Table IX. We investigate the contribution of multi-scale training strategy, we find that the multi-scale training strategy has little impact on the learning capability of the network, while only increase the IoU performance from 87.76 to 87.81 on GDD dataset [2]. Compared with multi-scale training strategy, IoU loss seems playing a vital role for boosting the performance. That's a misunderstanding because the IoU loss only has ability to optimize the IoU terms in evaluation metrics for our PGSNet, when it comes to F-measure and MAE metrics, IoU loss term enhances the performances slightly. Notably, the IoU loss does not always provide performance boosting. Another ablation study on IoU loss when training Trans2Seg [4] shows that the IoU metrics decrease from 84.4 to 83.66 on GDD [2] after increasing the auxiliary IoU loss.

TABLE IX
COMPARISON BETWEEN OUR PGSNET AND THE ONE TRAINING WITHOUT IOU LOSS OR WITHOUT MULTI-SCALE TRAINING STRATEGY.

Networks	GDD [2]			
	IoU \uparrow	$F_{\beta}^w\uparrow$	MAE \downarrow	BER \downarrow
Trans2Seg [4]	84.41	0.872	0.097	7.36
Trans2Seg [4] w/ IoU loss	83.66	0.863	0.083	7.67
PGSNet w/o IoU loss	86.97	0.898	0.066	6.04
PGSNet w/o multi-scale training strategy	87.76	0.899	0.061	5.68
PGSNet	87.81	0.901	0.062	5.56

H. Application to other tasks

With the help of the well-designed discriminability enhancement (DE) module and focus-and-exploration based fusion (FEFBF) module, our PGSNet can effectively fuse different levels of features, and thus has the potential to handle other challenging vision task. In this subsection, we consider three tasks, *i.e.*, transparency segmentation, mirror segmentation, and salient object detection, and conduct corresponding experiments to demonstrate the effectiveness and generalization capability of our proposed PGSNet.

1) *Transparency Segmentation*: Transparency segmentation aims to segment transparent regions in the scene. We retrain our PGSNet and conduct the performance evaluation on the Trans10K dataset [3] which contains both “Stuff” such as window, showcase, and glass guardrail, as well as “Things” such as eyeglass, cup, and bottle. We name the PGSNet retrained for transparency segmentation as PGSNet^T. We compare PGSNet^T with three state-of-the-art transparency/glass segmentation methods, including GDNNet [2], TransLab [3] and Trans2Seg [4], and report the quantitative comparison results in Table X. The superior results of our PGSNet^T clearly demonstrate the effectiveness of our method for transparency segmentation. Besides, by comparing the overall segmentation results in Table X and II, we can observe that the overall performance for both “Stuff” and “Things” segmentation is better than that of for “Stuff” only segmentation (*e.g.*, 89.35 versus 87.10 in terms of IoU for TransLab [3] on both “Stuff” and “Things” and “Stuff” only segmentation). This shows that the “Stuff” is more challenging than “Things” to be segmented. We think the reason is that the “Stuff” typically has a larger size and contains more diversity in patterns.

TABLE X
THE QUANTITATIVE EVALUATION ON THE TRANSPARENCY SEGMENTATION TASK.

Methods	Pub.'Year	Trans10K [3]			
		IoU \uparrow	$F_{\beta}^w\uparrow$	MAE \downarrow	BER \downarrow
GDNNet [2]	CVPR'20	91.72	0.933	0.027	3.04
TransLab [3]	ECCV'20	89.35	0.921	0.032	4.37
Trans2Seg [4]	IJCAI'21	91.14	0.932	0.027	3.33
PGSNet ^T	Ours	92.60	0.940	0.025	2.81

2) *Mirror Segmentation*: Mirror segmentation aims to segment regions that belong to the mirror. We retrain our PGSNet and conduct the performance evaluation on the MSD dataset [5] which is the first large-scale mirror segmentation dataset. We name the PGSNet retrained for mirror segmentation as PGSNet^M. We compare PGSNet^M with the state-of-the-art mirror segmentation method MirrorNet [5] and report the quantitative comparison results in Table XI. We can see that PGSNet^M performs favorably against MirrorNet [5]. Note that our PGSNet^M is an end-to-end process that does not need any post-processing, unlike MirrorNet [5] which require post-processing by a computationally costly fully connected conditional random field (CRF) [81].

3) *Salient Object Detection*: Salient object detection (SOD) is a fundamental yet challenging vision task which aims to highlight and segment the most visually distinctive objects in an input image. We retrain our PGSNet on DUTS-TR [88]

TABLE XI
THE QUANTITATIVE EVALUATION ON THE MIRROR SEGMENTATION TASK.

Methods	Backbone	MSD [5]			
		IoU \uparrow	$F_{\beta}^w\uparrow$	MAE \downarrow	BER \downarrow
MirrorNet [5]	ResNeXt-101	78.88	0.841	0.066	6.43
PGSNet ^M	ResNeXt-101	80.77	0.879	0.052	6.77

TABLE XII
THE QUANTITATIVE EVALUATION ON THE SALIENT OBJECT DETECTION TASK.

Methods	Backbone	DUT-OMRON [89]				DUTS-TE [88]			
		$S_{\alpha}\uparrow$	$E_{\phi}^a\uparrow$	$F_{\beta}^w\uparrow$	M \downarrow	$S_{\alpha}\uparrow$	$E_{\phi}^a\uparrow$	$F_{\beta}^w\uparrow$	M \downarrow
F3Net [31]	ResNet-50	.838	.870	.747	.053	.888	.902	.835	.035
MINet [26]	ResNet-50	.834	.866	.737	.056	.885	.899	.824	.037
ITSD [84]	ResNet-50	.840	.863	.750	.061	.885	.895	.824	.041
PGSNet ^S	ResNet-50	.839	.878	.758	.048	.889	.920	.849	.034

and conduct the performance evaluation on two challenging datasets, *i.e.*, DUT-OMRON [89] and DUTS-TE [88]. We name the PGSNet retrained for salient object detection as PGSNet^S. We compare PGSNet^S with three state-of-the-art SOD methods, including F3Net [31], MINet [26], and ITSD [84], and report the quantitative comparison results in Table XII. For a fair comparison, PGSNet^S adopts the same feature extractor (*i.e.*, ResNet-50 [87]) as three compared SOD methods. From the results, we can see that our PGSNet^S achieves comparable or even better performance than the compared methods in terms of four standard evaluation metrics, *i.e.*, structure-measure (S_{α}) [90], adaptive E-measure (E_{ϕ}^a) [91], weighted F-measure (F_{β}^w), and mean absolute error (M). This can be strong evidence to demonstrate the generalization capability of our method.

I. Discussion

1) *Negative examples*: We first curate 367 images without glass presence from the widely used publicly available dataset (*i.e.*, SUNRGBD [71]) and show some examples in Figure 10. Then we conduct experiments based on images with and without glass presence and report the corresponding results in Table XIII and Figure 11. We can see that introducing the images without glass into the training process will decrease the testing performance on images with glass to some extent but can significantly reduce the false positive predictions on images without glass presence. Note that only the MAE results are presented for images without glass as the other three metrics are not applicable for the all-zero ground truth map.

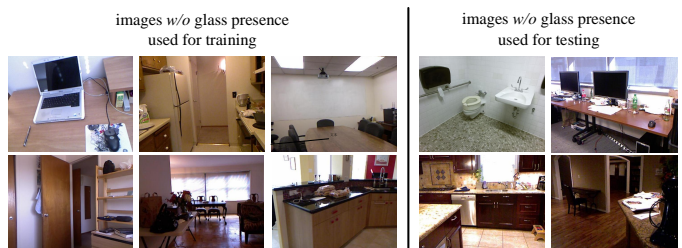


Fig. 10. Visual examples of our curated negative set (*i.e.*, images without glass presence).

TABLE XIII
THE QUANTITATIVE EVALUATION ON IMAGES w/ AND w/o GLASS.

Models	testing 1782 images w/ glass				testing 111 images w/o glass
	IoU \uparrow	$F_{\beta}^{w}\uparrow$	MAE \downarrow	BER \downarrow	MAE \downarrow
PGSNet trained on 3070 images w/ glass	80.06	0.836	0.089	9.08	0.304
PGSNet trained on 3070 images w/ glass + 256 images w/o glass	79.84	0.831	0.086	9.29	0.000

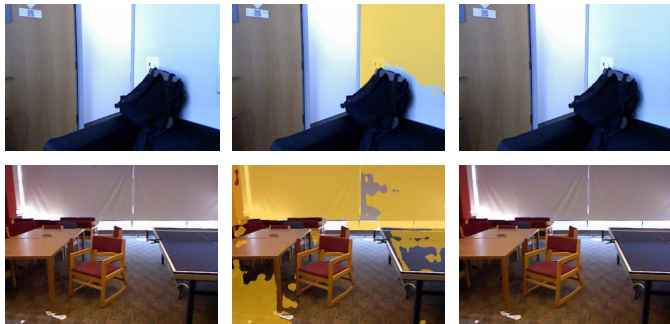


Image PGSNet trained on 3,070 images w/ glass PGSNet trained on 3,070 images w/ glass + 256 images w/o glass

Fig. 11. Our PGSNet trained with glass images only tends to over-segment the regions where perceptible boundary cues and highlights/reflections exist in the image without glass presence (e.g., the second column). Introducing the negative examples (i.e., images without glass presence) into the training process significantly reduces the false positive predictions (e.g., the third column).

2) *Limitation*: Note that the main focus of our work is about accuracy and our PGSNet is not a very efficient model. Besides, our method would fail in challenging scenes where both high-level and low-level features can not contribute strong cues for distinguishing glass and non-glass regions (e.g., as shown in Figure 12, floors and window screens in the house share similar high-level contextual relations and low-level boundary/reflection cues to the true glass regions, which makes our method output false positive predictions). A promising future research direction is to explore multi-view cues for robust glass segmentation in such complex scenes.

3) *Future work*: Our future work is three-fold. First, our PGSNet still has a burden on computational efficiency, and it will be a great improvement by simplifying the PGSNet. Second, as the reflection information, a crucial cue for glass segmentation may be more obvious in the video, we are interested in glass segmentation in video fields. Finally, existing glass segmentation data is only based on static images. However, glass segmentation in other modalities (e.g., event data or depth information) raises new challenges under specific scenes.

V. CONCLUSION

In this paper, we strive to embrace challenges in level-different features fusion towards accurate glass segmentation. We develop a novel feature fusion strategy for richly excavating useful information via both focus and exploration between features. By adopting this strategy in our progressive glass segmentation network (PGSNet), we show that



Fig. 12. Failure case. Our method would fail to segment glass in some complex scenes where both high-level and low-level features can not contribute strong cues for distinguishing glass and non-glass regions. In this case, floors and window screens in the house share similar high-level contextual relations and low-level boundary/reflection cues to the true glass regions, which makes our level-different features fusion based method naturally generate sub-optimal glass segmentation results.

our approach achieves state-of-the-art performance on two benchmark datasets as well as our home-scene-oriented (HSO) glass segmentation dataset. In the future, we plan to explore the potential of our method for other applications such as material segmentation and further enhance its capability for segmenting glass in videos.

ACKNOWLEDGMENT

This work was supported in part by the National Natural Science Foundation of China under Grant 61972067/U21A20491/U1908214, National Key Research and Development Program of China (2021ZD0112400), and the Innovation Technology Funding of Dalian (2020JJ26GX036).

REFERENCES

- [1] T. Whelan, M. Goesele, S. Lovegrove, J. Straub, S. Green, R. Szeliski, S. Butterfield, S. Verma, and R. Newcombe, "Reconstructing scenes with mirror and glass surfaces," *ACM TOG*, 2018.
- [2] H. Mei, X. Yang, Y. Wang, Y. Liu, S. He, Q. Zhang, X. Wei, and R. W. Lau, "Don't hit me! glass detection in real-world scenes," in *CVPR*, 2020.
- [3] E. Xie, W. Wang, W. Wang, M. Ding, C. Shen, and P. Luo, "Segmenting transparent objects in the wild," in *ECCV*, 2020.
- [4] E. Xie, W. Wang, W. Wang, P. Sun, H. Xu, D. Liang, and P. Luo, "Segmenting transparent object in the wild with transformer," in *IJCAI*, 2021.
- [5] X. Yang, H. Mei, K. Xu, X. Wei, B. Yin, and R. W. Lau, "Where is my mirror?" in *ICCV*, 2019.
- [6] A. Vaswani, N. Shazeer, N. Parmar, J. Uszkoreit, L. Jones, A. N. Gomez, L. Kaiser, and I. Polosukhin, "Attention is all you need," in *NeurIPS*, 2017.
- [7] J. Long, E. Shelhamer, and T. Darrell, "Fully convolutional networks for semantic segmentation," in *CVPR*, 2015.
- [8] L.-C. Chen, G. Papandreou, I. Kokkinos, K. Murphy, and A. L. Yuille, "Deeplab: Semantic image segmentation with deep convolutional nets, atrous convolution, and fully connected crfs," *IEEE TPAMI*, 2017.
- [9] J. Fu, J. Liu, H. Tian, Y. Li, Y. Bao, Z. Fang, and H. Lu, "Dual attention network for scene segmentation," in *CVPR*, 2019.
- [10] Z. Huang, X. Wang, L. Huang, C. Huang, Y. Wei, and W. Liu, "Ccnct: Criss-cross attention for semantic segmentation," in *ICCV*, 2019.
- [11] M. Yang, K. Yu, C. Zhang, Z. Li, and K. Yang, "Denseaspp for semantic segmentation in street scenes," in *CVPR*, 2018.
- [12] C. Yu, J. Wang, C. Peng, C. Gao, G. Yu, and N. Sang, "Bisenet: Bilateral segmentation network for real-time semantic segmentation," in *ECCV*, 2018.
- [13] H. Zhang, K. Dana, J. Shi, Z. Zhang, X. Wang, A. Tyagi, and A. Agrawal, "Context encoding for semantic segmentation," in *CVPR*, 2018.
- [14] H. Zhao, J. Shi, X. Qi, X. Wang, and J. Jia, "Pyramid scene parsing network," in *CVPR*, 2017.
- [15] H. Zhao, Y. Zhang, S. Liu, J. Shi, C. Change Loy, D. Lin, and J. Jia, "Psanet: Point-wise spatial attention network for scene parsing," in *ECCV*, 2018.

- [16] X. Li, A. You, Z. Zhu, H. Zhao, M. Yang, K. Yang, S. Tan, and Y. Tong, "Semantic flow for fast and accurate scene parsing," in *ECCV*, 2020.
- [17] X. Li, H. Zhao, L. Han, Y. Tong, S. Tan, and K. Yang, "Gated fully fusion for semantic segmentation," *AAAI*, 2020.
- [18] S. Huang, Z. Lu, R. Cheng, and C. He, "FaPN: Feature-aligned pyramid network for dense image prediction," in *ICCV*, 2021.
- [19] S. Minaee, Y. Y. Boykov, F. Porikli, A. J. Plaza, N. Kehtarnavaz, and D. Terzopoulos, "Image segmentation using deep learning: A survey," *IEEE TPAMI*, 2021.
- [20] R. Achanta, S. Hemami, F. Estrada, and S. Susstrunk, "Frequency-tuned salient region detection," in *CVPR*, 2009.
- [21] M.-M. Cheng, N. J. Mitra, X. Huang, P. H. Torr, and S.-M. Hu, "Global contrast based salient region detection," *IEEE TPAMI*, 2014.
- [22] G. Lee, Y.-W. Tai, and J. Kim, "Deep saliency with encoded low level distance map and high level features," in *CVPR*, 2016.
- [23] Q. Hou, M.-M. Cheng, X. Hu, A. Borji, Z. Tu, and P. Torr, "Deeply supervised salient object detection with short connections," *IEEE TPAMI*, 2019.
- [24] P. Zhang, D. Wang, H. Lu, H. Wang, and X. Ruan, "Amulet: Aggregating multi-level convolutional features for salient object detection," in *ICCV*, 2017.
- [25] T. Zhao and X. Wu, "Pyramid feature attention network for saliency detection," in *CVPR*, 2019.
- [26] Y. Pang, X. Zhao, L. Zhang, and H. Lu, "Multi-scale interactive network for salient object detection," in *CVPR*, 2020.
- [27] H. Mei, Y. Liu, Z. Wei, D. Zhou, X. Wei, Q. Zhang, and X. Yang, "Exploring dense context for salient object detection," *IEEE TCSVT*, 2021.
- [28] X. Zhang, T. Wang, J. Qi, H. Lu, and G. Wang, "Progressive attention guided recurrent network for salient object detection," in *CVPR*, 2018.
- [29] Z. Deng, X. Hu, L. Zhu, X. Xu, J. Qin, G. Han, and P.-A. Heng, "R3net: Recurrent residual refinement network for saliency detection," in *IJCAI*, 2018.
- [30] W. Wang, J. Shen, M.-M. Cheng, and L. Shao, "An iterative and cooperative top-down and bottom-up inference network for salient object detection," in *CVPR*, 2019.
- [31] J. Wei, S. Wang, and Q. Huang, "F3net: Fusion, feedback and focus for salient object detection," *AAAI*, 2020.
- [32] N. Liu, J. Han, and M.-H. Yang, "Picanet: Learning pixel-wise contextual attention for saliency detection," in *CVPR*, 2018.
- [33] S. Chen, X. Tan, B. Wang, and X. Hu, "Reverse attention for salient object detection," in *ECCV*, 2018.
- [34] Z. Wu, L. Su, and Q. Huang, "Cascaded partial decoder for fast and accurate salient object detection," in *CVPR*, 2019.
- [35] X. Tian, K. Xu, X. Yang, B. Yin, and R. W. Lau, "Weakly-supervised salient instance detection," in *Bmvc*, 2020.
- [36] X. Tian, K. Xu, X. Yang, B. Yin, and R. W. Lau, "Learning to detect instance-level salient objects using complementary image labels," *IJCV*, 2021.
- [37] X. Qin, Z. Zhang, C. Huang, C. Gao, M. Dehghan, and M. Jagersand, "Basnet: Boundary-aware salient object detection," in *CVPR*, 2019.
- [38] J.-J. Liu, Q. Hou, M.-M. Cheng, J. Feng, and J. Jiang, "A simple pooling-based design for real-time salient object detection," in *CVPR*, 2019.
- [39] J.-X. Zhao, J.-J. Liu, D.-P. Fan, Y. Cao, J. Yang, and M.-M. Cheng, "Egnet: edge guidance network for salient object detection," in *ICCV*, 2019.
- [40] W. Wang, J. Shen, X. Dong, A. Borji, and R. Yang, "Inferring salient objects from human fixations," *IEEE TPAMI*, 2019.
- [41] W. Wang, S. Zhao, J. Shen, S. C. Hoi, and A. Borji, "Salient object detection with pyramid attention and salient edges," in *CVPR*, 2019.
- [42] W. Wang, Q. Lai, H. Fu, J. Shen, H. Ling, and R. Yang, "Salient object detection in the deep learning era: An in-depth survey," *IEEE TPAMI*, 2021.
- [43] D.-P. Fan, J. Zhang, G. Xu, M.-M. Cheng, and L. Shao, "Salient objects in clutter," *arXiv:2105.03053*, 2021.
- [44] X. Hu, L. Zhu, C.-W. Fu, J. Qin, and P.-A. Heng, "Direction-aware spatial context features for shadow detection," in *CVPR*, 2018.
- [45] H. Le, T. F. Yago Vicente, V. Nguyen, M. Hoai, and D. Samaras, "A+d net: Training a shadow detector with adversarial shadow attenuation," in *ECCV*, 2018.
- [46] L. Zhu, Z. Deng, X. Hu, C.-W. Fu, X. Xu, J. Qin, and P.-A. Heng, "Bidirectional feature pyramid network with recurrent attention residual modules for shadow detection," in *ECCV*, 2018.
- [47] Q. Zheng, X. Qiao, Y. Cao, and R. W. Lau, "Distraction-aware shadow detection," in *CVPR*, 2019.
- [48] X. Han, C. Nguyen, S. You, and J. Lu, "Single image water hazard detection using fcn with reflection attention units," in *ECCV*, 2018.
- [49] X. Yang, K. Xu, S. Chen, S. He, B. Y. Yin, and R. Lau, "Active matting," in *NeurIPS*, 2018.
- [50] H. Mei, B. Dong, W. Dong, P. Peers, X. Yang, Q. Zhang, and X. Wei, "Depth-aware mirror segmentation," in *CVPR*, 2021.
- [51] J. Lin, Z. He, and R. W. Lau, "Rich context aggregation with reflection prior for glass surface detection," in *CVPR*, 2021.
- [52] H. He, X. Li, G. Cheng, J. Shi, Y. Tong, G. Meng, V. Prinet, and L. Weng, "Enhanced boundary learning for glass-like object segmentation," in *ICCV*, 2021.
- [53] X. Yang, H. Mei, J. Zhang, K. Xu, B. Yin, Q. Zhang, and X. Wei, "Drfn: Deep recurrent fusion network for single-image super-resolution with large factors," *IEEE TMM*, 2018.
- [54] J. Zhang, C. Long, Y. Wang, X. Yang, H. Mei, and B. Yin, "Multi-context and enhanced reconstruction network for single image super resolution," in *ICME*, 2020.
- [55] J. Zhang, C. Long, Y. Wang, H. Piao, H. Mei, X. Yang, and B. Yin, "A two-stage attentive network for single image super-resolution," *IEEE TCSVT*, 2021.
- [56] Y. Qiao, Y. Liu, Q. Zhu, X. Yang, Y. Wang, Q. Zhang, and X. Wei, "Multi-scale information assembly for image matting," in *Computer Graphics Forum*, 2020.
- [57] Y. Liu, J. Xie, X. Shi, Y. Qiao, Y. Huang, Y. Tang, and X. Yang, "Tripartite information mining and integration for image matting," in *ICCV*, 2021.
- [58] Y. Liu, J. Xie, Y. Qiao, Y. Tang, and X. Yang, "Prior-induced information alignment for image matting," *IEEE TMM*, 2021.
- [59] H. Mei, G.-P. Ji, Z. Wei, X. Yang, X. Wei, and D.-P. Fan, "Camouflaged object segmentation with distraction mining," in *CVPR*, 2021.
- [60] Y. Qiao, Y. Liu, X. Yang, D. Zhou, M. Xu, Q. Zhang, and X. Wei, "Attention-guided hierarchical structure aggregation for image matting," in *CVPR*, 2020.
- [61] S. Xie, R. Girshick, P. Dollár, Z. Tu, and K. He, "Aggregated residual transformations for deep neural networks," in *CVPR*, 2017.
- [62] S. Liu, D. Huang, and a. Wang, "Receptive field block net for accurate and fast object detection," in *ECCV*, 2018.
- [63] Y. Pang, Y. Li, J. Shen, and L. Shao, "Towards bridging semantic gap to improve semantic segmentation," in *CVPR*, 2019.
- [64] J. Hu, L. Shen, and G. Sun, "Squeeze-and-excitation networks," in *CVPR*, 2018.
- [65] H. Ding, X. Jiang, B. Shuai, A. Q. Liu, and G. Wang, "Context contrasted feature and gated multi-scale aggregation for scene segmentation," in *CVPR*, 2018.
- [66] X. Li, X. Li, L. Zhang, G. Cheng, J. Shi, Z. Lin, S. Tan, and Y. Tong, "Improving semantic segmentation via decoupled body and edge supervision," in *ECCV*, 2020.
- [67] P.-T. De Boer, D. P. Kroese, S. Mannor, and R. Y. Rubinstein, "A tutorial on the cross-entropy method," in *Annals of Operations Research*, 2005.
- [68] G. Mattyas, W. Luo, and R. Urtasun, "Deeproadmapper: Extracting road topology from aerial images," in *ICCV*, 2017.
- [69] S. Xie and Z. Tu, "Holistically-nested edge detection," in *ICCV*, 2015.
- [70] A. Chang, A. Dai, T. Funkhouser, M. Halber, M. Niessner, M. Savva, S. Song, A. Zeng, and Y. Zhang, "Matterport3D: Learning from RGB-D data in indoor environments," in *3DV*, 2017.
- [71] S. Song, S. P. Lichtenberg, and J. Xiao, "Sun rgb-d: A rgb-d scene understanding benchmark suite," in *CVPR*, 2015.
- [72] A. Dai, A. X. Chang, M. Savva, M. Halber, T. Funkhouser, and M. NieBner, "ScanNet: Richly-annotated 3d reconstructions of indoor scenes," in *CVPR*, 2017.
- [73] I. Armeni, S. Sax, A. R. Zamir, and S. Savarese, "Joint 2d-3d-semantic data for indoor scene understanding," *arXiv:1702.01105*, 2017.
- [74] R. Margolin, L. Zelnik-Manor, and A. Tal, "How to evaluate foreground maps?" in *CVPR*, 2014.
- [75] V. Nguyen, T. F. Yago Vicente, M. Zhao, M. Hoai, and D. Samaras, "Shadow detection with conditional generative adversarial networks," in *ICCV*, 2017.
- [76] D.-P. Fan, M.-M. Cheng, Y. Liu, T. Li, and A. Borji, "Structure-measure: A new way to evaluate foreground maps," in *ICCV*, 2017.
- [77] D.-P. Fan, C. Gong, Y. Cao, B. Ren, M.-M. Cheng, and A. Borji, "Enhanced-alignment measure for binary foreground map evaluation," *IJCAI*, 2018.
- [78] A. Paszke, S. Gross, F. Massa, A. Lerer, J. Bradbury, G. Chanan, T. Killeen, Z. Lin, N. Gimelshein, L. Antiga *et al.*, "Pytorch: An imperative style, high-performance deep learning library," in *NeurIPS*, 2019.
- [79] J. Deng, W. Dong, R. Socher, L.-J. Li, K. Li, and L. Fei-Fei, "Imagenet: A large-scale hierarchical image database," in *CVPR*, 2009.

- [80] W. Liu, A. Rabinovich, and A. C. Berg, "Parsenet: Looking wider to see better," *arXiv:1506.04579*, 2015.
- [81] P. Krähenbühl and V. Koltun, "Efficient inference in fully connected crfs with gaussian edge potentials," in *NeurIPS*, 2011.
- [82] H. Zhao, X. Qi, X. Shen, J. Shi, and J. Jia, "Icnet for real-time semantic segmentation on high-resolution images," in *ECCV*, 2018.
- [83] L.-C. Chen, Y. Zhu, G. Papandreou, F. Schroff, and H. Adam, "Encoder-decoder with atrous separable convolution for semantic image segmentation," in *ECCV*, 2018.
- [84] H. Zhou, X. Xie, J.-H. Lai, Z. Chen, and L. Yang, "Interactive two-stream decoder for accurate and fast saliency detection," in *CVPR*, 2020.
- [85] D.-P. Fan, G.-P. Ji, T. Zhou, G. Chen, H. Fu, J. Shen, and L. Shao, "Pranet: Parallel reverse attention network for polyp segmentation," *MICCAI*, 2020.
- [86] K. Simonyan and A. Zisserman, "Very deep convolutional networks for large-scale image recognition," *arXiv:1409.1556*, 2014.
- [87] K. He, X. Zhang, S. Ren, and J. Sun, "Deep residual learning for image recognition," in *CVPR*, 2016.
- [88] L. Wang, H. Lu, Y. Wang, M. Feng, D. Wang, B. Yin, and X. Ruan, "Learning to detect salient objects with image-level supervision," in *CVPR*, 2017.
- [89] C. Yang, L. Zhang, H. Lu, X. Ruan, and M.-H. Yang, "Saliency detection via graph-based manifold ranking," in *CVPR*, 2013.
- [90] D.-P. Fan, M.-M. Cheng, Y. Liu, T. Li, and A. Borji, "Structure-measure: A new way to evaluate foreground maps," in *ICCV*, 2017.
- [91] D.-P. Fan, C. Gong, Y. Cao, B. Ren, M.-M. Cheng, and A. Borji, "Enhanced-alignment measure for binary foreground map evaluation," in *IJCAI*, 2018.



Ziqi Wei received the BS degree in computing science and technology from Renmin University of China, in June 2009 and the Ph.D. degree from University of Alberta, in Nov 2018. He is doing his post doc research in Tsinghua University. His research areas include wireless sensor network, computing theory, heuristic algorithms, health ageing and big data techniques in health care.



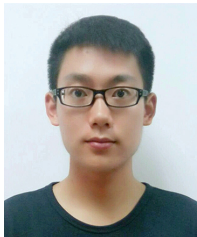
Li Zhu received the B.E. degree in automation from Dalian University of Technology, Dalian, China, in 2009, and the Ph.D. degree in control science and engineering from Zhejiang University, Hangzhou, China, in 2014. He is currently an Assistant Professor with the School of Control Science and Engineering, Dalian University of Technology, Dalian, China. His current research interests include data mining and analytics, process monitoring and diagnosis, machine intelligence, and knowledge automation.



Letian Yu is a Ph.D. student in the School of Computer Science at Dalian University of Technology. He received his B.S. degree in Computer Science and Technology in 2019. His research interests are computer vision and image processing.



Yuxin Wang received the MS degree in Computer Application in 2000 and the PhD degree in Computer Science in 2012 from Dalian University of Technology, P.R. China. He is currently an Associate Professor in the College of Computer Science at Dalian University of Technology. His research interests include distributed computing, big data analysis, deep learning and computer vision.



Haiyang Mei received the B.Eng. degree in the Automation from Dalian University of Technology, Dalian China, in 2017. He is currently working toward the Ph.D. degree with the School of Computer Science and Technology, Dalian University of Technology, Dalian, China. His research interests include image processing and computer vision.



Xin Yang is a Professor in the Department of Computer Science at Dalian University of Technology, China. Yang received his B.S. degree in Computer Science from Jilin University in 2007. From 2007 to June 2012, he was a joint Ph.D. student at Zhejiang University and UC Davis for Graphics and received his Ph.D. degree in July 2012. His research interests include computer graphics and robotic vision.



Wen Dong received his bachelor's degree in software engineering from Northwest A & F University in 2019 and now is studying for a master's degree in the School of Computer Science and Technology at Dalian University of Technology. His research interests are computer vision and image processing.